Chaos in Seemingly Simple Optical Systems *LiamPacker*

1 Abstract

A particularly illuminating application of analysis in dynamical systems is to that of (nonlinear) optical systems. These systems are characterized by a nonlinear response of a material by an incident electromagnetic wave, allowing for the existence of a variety of phenomena such as laser pumping, frequency-doubling, four-wave-mixing, and many more [6]. What is less well known is that chaotic behavior can emerge in even the simplest of these systems. Both in optical pumping and nonlinear wave propagation, it was predicted that chaotic behavior was possible and emergent when a particular set of conditions are met depending on the system. As an example, in the simple case of optical pumping of a nonlinear gain material, the system can be modeled by a set of equations known as the Maxwell-Bloch equations [3] which bear striking similarity to the Lorenz system (and in fact, reduce to the Lorenz system under certain conditions on the parameters). We'll be analyzing a different, but still seemingly simple, optical system known as the ring cavity with a dielectric medium. We will be following [5] and [4] closely. It has been shown [5] that under reasonable boundary conditions on the ring, the dynamics of the system are given by the difference-differential equations

$$\begin{aligned} E(t) &= A + BE(t - t_R)\exp\{i[\phi(t) - \phi_0]\}, \\ \gamma^{-1}\dot{\phi}(t) &= -\phi(t) + \text{sgn}(n_2)|E(t - t_R)|^2 \end{aligned}$$

where γ is a relaxation rate parameter, A is proportional to the amplitude of the incident field, B characterizes the dissipation of the electric field through the cavity, and t_R a time delay. This complex map can be reduced to a one-dimensional real map by considering instead the intensity $I \propto |E|^2$, which [3] showed to be:

$$I_{n+1} = I_{in}\left(1 + C\cos\left(\frac{2\pi L}{\lambda}(n_2 I_n + \phi_0)\right)\right)$$

Variation of the parameters A, B, ϕ_0, and C will yield different possible steady-state solutions. As the steady-state solutions become unstable through the variation in parameters, the system undergoes a sequence of bifurcations eventually yielding a chaotic regime with an associated strange

attractor [4]. We will calculate the fractal dimension for some of these strange attractors in the chaotic regime. We will also do analysis in the one-dimensional real map, which will reveal a period-doubling sequence akin to the logistic map's road to chaos, followed by sets of chaotic regimes [3], along with other surprises which we will discover for the first time below.

2 A Brief Introduction to Nonlinear Optics

2.1 Nonlinear Polarization

First, we will get at taste of how higher-order dependence of a dielectric medium on an electric field can produce interesting effects, especially the effect of an intensity-dependent index of refraction. This will be key in the model we will study, for this nonlinear response of the medium in the presence of an electric field will pave the way for a road to chaos.

In typical optics, we consider a dielectric material which has a *linear* relationship with incident electromagnetic waves. For simplicity, we consider only the electric field. We say that a material is *polarized* when, in a classical approximation, an electric field aligns the molecular dipoles of the material in a certain direction. The direction of polarization is in general dependent on the shape of material, type of material, position in the material, and the frequency and strength of the incident electric field. In the simplest model, we assume that the reaction of the material's molecular dipole moment density $\mathbf{P}$ is *linear* in the electric field strength, $\mathbf{P} \propto \mathbf{E}$, where $\mathbf{P} \equiv$ "average dipole moment" for a very small region of space. In a first course of electromagnetics, the proportionality is taken to be direct, so that $\mathbf{P} = \epsilon_0 \chi_e \mathbf{E}$, where χ_e is known as the "electric susceptibility" of the medium [2] and quantifies how strong the reaction of the molecules in the material is to the incident electric field. In general, the relationship can be true up to a linear transformation, so that $\mathbf{P} = \epsilon_0 \chi^{(1)}(\mathbf{E})$, where $\chi^{(1)}$ is known as the first-order (or linear) susceptibility, a linear map defined at each point in the dielectric medium [2]. This first-order tensor allows for the medium to prefer certain polarization directions at different locations, although the relationship is still linear and involves only first "powers" of $\mathbf{E}$. This linear relationship means that the resulting *intensity* of the total electric field in the medium can only be linear in the incident electric field intensity.

Next, we introduce nonlinearities in the dependence of the polarization

$\mathbf{P}$ on the electric field $\mathbf{E}$ by expanding $\mathbf{P}$ as a power-series in higher-order susceptibility tensors [1]:

$$\begin{aligned}\mathbf{P} &= \epsilon_0[\chi^{(1)}(\mathbf{E}) + \chi^{(2)}(\mathbf{E},\mathbf{E}) + \chi^{(3)}(\mathbf{E},\mathbf{E},\mathbf{E}) + \cdots] \\ &= \mathbf{P}^{(1)} + \mathbf{P}^{(2)} + \mathbf{P}^{(3)} + \cdots,\end{aligned}$$

where we define the n^{th} order polarization to be $\mathbf{P}^{(n)} = \chi^{(n)}(\mathbf{E},\cdots,\mathbf{E})$. In more typical component notation, the n^{th} order polarization component P^i can be written as $P^i = \sum_{j,k,\cdots} \chi^{(n)}_{ij\cdots} E^j E^k \cdots$. We can immediately see the nonlinear dependence of $\mathbf{P}$ on $\mathbf{E}$ through the products of components E^j proportioned by $\chi_{ij\cdots}$. We note that the polarization $\mathbf{P}$, in this approximation, only depends on the electric field at the *current time* t, $\mathbf{E}(t)$. Physically this means the medium responds instantaneously to the electric field, which we'll assume from here on out. In general the dependence is non-instantaneous in the case of materials with dispersion or loss [1].

2.2 Intensity-Dependent Refractive Index

For simplicity, we drop the tensors and consider the polarization magnitude and electric field magnitude. The third-order polarization magnitude $P^{(3)}(t)$ is then expressed as $P^{(3)}(t) = \epsilon_0\chi^{(3)}E^3(t) \propto E^3(t)$, where $\chi^{(3)}$ is now a *scalar*, meaning P is linearly dependent on the cube of E. If we assume a monochromatic wave, $E(t) = \mathcal{E}\cos\omega t$, then using the identity $\cos^3\omega t = \frac{1}{4}\cos(3\omega t) + \frac{3}{4}\cos\omega t$:

$$P^{(3)}(t) = \frac{1}{4}\epsilon_0\chi^{(3)}\mathcal{E}^3\cos 3\omega t + \frac{3}{4}\epsilon_0\chi^{(3)}\mathcal{E}^3\cos\omega t.$$

We can see that two frequency terms emerge: a component with frequency 3ω, known as the third-harmonic generated component, and a component with the original frequency ω which gives rise to an intensity-dependent index of refraction. This intensity-dependent effect is exactly what we needed. Writing the index of refraction as a function of frequency, $n(\omega)$ is a known function of χ when magnetization can be neglected: $n(\omega) = \sqrt{1+\chi_{eff}(\omega)}$, where $\chi_{eff}(\omega)$ is the proportionality between $E(\omega)$ and $P(\omega)$. For our case, E has a single frequency component ω and P has two frequency components, 3ω and ω. As a result, since $P(\omega) = \epsilon_0[\chi^{(1)}E(\omega) + 3\chi^{(3)}|E(\omega)|^2E(\omega)]$, we can see that $\chi_{eff} = \chi^{(1)} + 3\chi^{(3)}|E(\omega)|^2$. Since the intensity $I(\omega)$ is proportional

to the squared magnitude of the electric field $|E(\omega)|^2$, we can see that $n(\omega) = n_0 + n_2 I(\omega)$ when we neglect higher order terms than $|E(\omega)|^2$, where n_2 is a constant determined by the above factors [1].

2.3 A Simple System and Some Intuition

The simple system we wish to analyze is the well-known ring resonator with a single gain medium along one branch of the ring, see figure 1. Light is input from the outside where the light beam then travels along the ring, guided by the mirrors. Of interest is the lights interaction with the gain medium, where there is opportunity for amplification and phase shift of the incoming light. In this way the gain medium acts as a pump for the incoming light, so that the outgoing light's intensity can be larger than the input intensity. Yet with the nonlinear nature of the gain medium, the outgoing light's spectrum may also be different due to the possibility of higher frequency generation, as we saw with the third-order polarization.

Intuitively, we can see that the cavity length, L will have an effect on the phase shift of the incoming light on a single round-trip even in the linear case. Since light propagates at a different speed in the medium and at the same speed in the other three branches, we'll have a phase shift (after one round trip) of $\phi_0 = (2\pi/\lambda)L \cdot n_0$ for a given frequency $\omega = 2\pi/\lambda$. Since we saw above that the index of refraction is intensity-dependent in the third-order nonlinear case, we have to modify this phase shift to $\phi = (2\pi/\lambda)L \cdot n(I) = (2\pi/\lambda)L \cdot (n_0 + n_2 I)$.

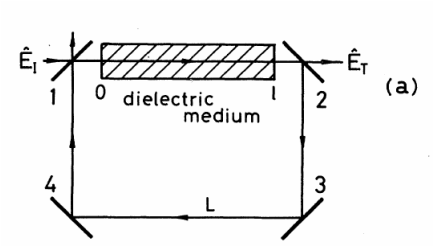

Figure 1: From [4], a schematic of the ring-resonator used to demonstrate chaotic behavior in a simple optical system.

3 Analysis

We'll be following and expanding upon some of the analysis of the above system in [3] and [4]. We'll also fill in the gaps in going from the analysis of the system in [4] to [3] which were very largely left out in the discussion. We'll see the extent to which the nonlinear nature of the gain medium effects the evolution of the electric field intensity and when chaos sets in.

We'll start with a result derived in [5] and utilized in [4], namely the equations which determine the evolution of an incident monochromatic light beam around the ring resonator including the field amplitude and phase shift:

$$E(t) = A + BE(t - t_R)\exp\{i[\phi(t) - \phi_0]\}, \tag{1}$$

$$\gamma^{-1}\dot{\phi}(t) = -\phi(t) + \text{sgn}(n_2)|E(t - t_R)|^2. \tag{2}$$

These equations are arrived at in [5] through the Maxwell-Debye equations which govern the propagation of light in a two-level system when the system is "homogeneously broadened," and the details are beyond the scope of this paper.

Now to describe the physical meaning of some parameters. First, $E(t)$ is a dimensionless form of the electric field amplitude at the ring's top-left corner, where distance is measured around the circle starting from the top-left corner and wrapping around after the entire ring is traversed. Importantly, $E(t) \propto \sqrt{(2\pi/\lambda)n_2}$. n_2 is the nonlinear refractive instance we arrived at above, $\phi(t)$ is the phase shift suffered by the electric field in the medium, ϕ_0 is the mismatch of the cavity's length with the light's wavelength (as above, $\phi_0 = (2\pi/\lambda)n_0$, γ is a measure of the relaxation rate of the phase shift. A is proportional to the amplitude of the incident electric field, and B characterizes the dissipation of the electric field in the cavity. Importantly, $A \propto \sqrt{(2\pi/\lambda)n_2}E_I$, the incident electric field. t_R is a time delay from the propagation of light through the medium, $t_R = L/c$. We can see that the electric field amplitude $E(t_0)$ at some time t_0 will depend only on the electric field before the last "round trip" of the light, $t_0 - t_R$ when ignoring the vacuum regions of the cavity. Since the refractive index is 0 in a vacuum, the gain medium produces all effects on the electric field and time-differences can be taken relative to the end-points of the medium.

To analyze this system we'll assume that we reach a steady-state in the phase shift $\dot{\phi}(t) = 0$ so that $\phi(t) = \text{sgn}(n_2)|E(t - t_R)|^2$, or alternatively that $\gamma t_R \to \infty$. Then we have that $E(t) = A + BE(t - t_R)\exp\{i[\text{sgn}(n_2)|E(t -$

$t_R)|^2 - \phi_0]\}$. Multiplying both sides by E_{in}, normalizing, and assuming n_2 is *negative*, we can again re-write:

$$\begin{aligned} E(t) &= A + BE(t - t_R)\exp\{i[-|E(t - t_R)|^2 - \phi_0]\} \\ \Rightarrow E(t)I_{in} &= A \cdot E_{in} + B \cdot I_{in}E(t - t_R)\exp\{i[-|E(t - t_R)|^2 - \phi_0]\} \\ \Rightarrow \tilde{I}(t) &= \tilde{I}_{in}(1 + C\exp\{-i(n_2\tilde{I}(t - t_R) - \phi_0)\}) \end{aligned}$$

(Author's Note: We cheated in the above and simply re-assigned $E(t)\cdot E_{in} \rightarrow I(t)$ for each occurrence, since I don't see a physical way that [3] arrived at its central equation other than by this kind of re-labeling. What should have happened is that an equation for intensity should have fallen out after multiplying both sides of $E(t)$ by its complex conjugate, but this introduces cross terms not included in [3], so I left them out in favor of sticking with the literature. I suspect this could have been a mistake).

Taking the real part of both sides we arrive at the central one-dimensional mapping analyzed in [3], re-label $\tilde{I} \rightarrow I$, utilizing the fact that $\cos(\theta) = \cos(-\theta)$ and letting $I_n = I(nt_R)$:

$$I_{n+1} = I_{in}\left(1 + C\cos\left[\frac{2\pi L}{\lambda}n_2 I_n + \phi_0\right]\right) \tag{3}$$

Notice that when nonlinear effects can be neglected ($n_2 = 0$), $I_{n+1} = I_{in}(1 + C\cos\phi_0)$, which is the result from linear optics of light being continually pumped by a gain medium through a ring resonator, which is reassuring.

The steady-state solution I_s can be reached by solving $I_s = I_{in}(1 + C\cos(\frac{2\pi L}{\lambda}n_2 I_s + \phi_0))$, but we won't get much further than that. The result is a globally stable fixed point which we can see from figure 2.

Finally, in [3], they simply state that "the Liapunov exponent" is $\log\frac{I_{in}C}{2}$, for which chaos occurs when $I_{in}C > 2$, but this cannot be the case since a single Liapunov exponent doesn't globally apply to the system unless there is a single globally attracting trajectory. Furthermore, the Liapunov exponent calculated in the below changes significantly depending on the trajectory and type of trajectory. We also found stable trajectories on cycles for $I_{in}C > 2$, in the case $I_{in} = 1$. Finally, we'll see in the next section that there are sometimes *two stable trajectory types*, for which the Liapunov exponent is *different*. This seems to have been another oversight in [3].

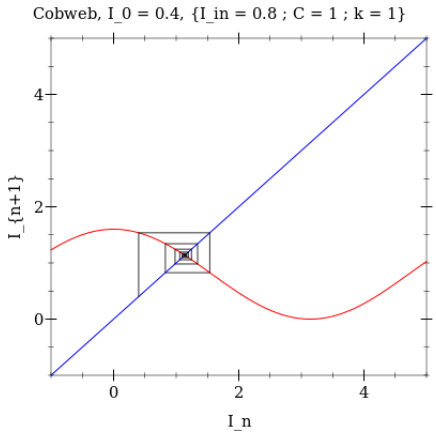

Figure 2: Cobweb diagram of the intensity map with a globally stable solution. The Liapunov exponent is calculated empirically to be $\lambda \approx -0.3205$, indicating nearby neighborhoods shrinking towards it throughout any starting trajectory

3.1 The Journey to Chaos

We can see qualitatively, as we increase C from 1.0, a series of period doubling occurs, examples of which are shown in figure 3. Each of these cycles has a negative Liapunov exponent and a derivative with magnitude less than one, calculated as a product of the derivative of each point in the cycle.

3.2 Chaos

The sequence of period doubling roughly continues until chaos occurs at some threshold C value. We can see from figure 4 that chaotic behavior characteristic of an unstable-everywhere map occurs, reminiscent of the logistic map above its critical control value r_c. This chaotic behavior continues, but we also encounter brief periods of periodic behavior much like in the case of the logistic map. To get a better idea of how the global dynamics evolve with C, we continue with an orbit diagram, something which wasn't calculated in neither [3] nor [4], but which shines a very bright light on the behavior of this map.

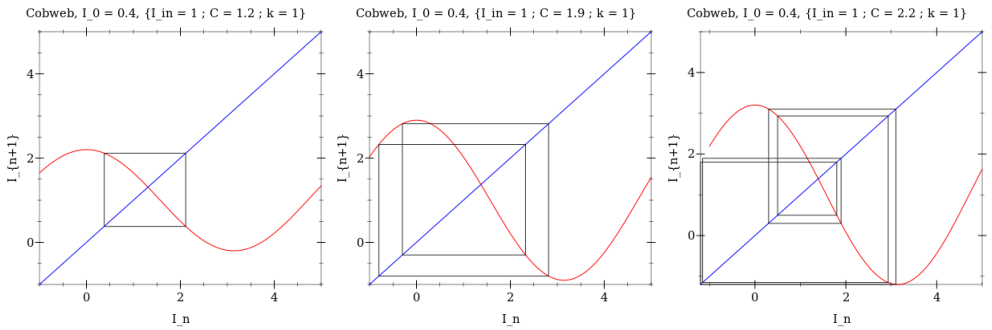

Figure 3: A representative set of cobwebs of the I_{n+1} map's period doubling phenomena for C increasing above 1.0. The Liapunov exponent is calculated empirically to be negative for each trajectory ($\lambda \approx -0.10966, -0.39309, -0.08662$ for the 2-cycle, 4-cycle, and 8-cycle respectively). We also calculated the derivative products on each trajectory's cycle points to be less than one, indicating these cycles are, in fact, stable ($\Pi_i f'(x_i) = 0.64491, 0.45558, 0.50001$ for the 2-cycle, 4-cycle, and 8-cycle respectively).

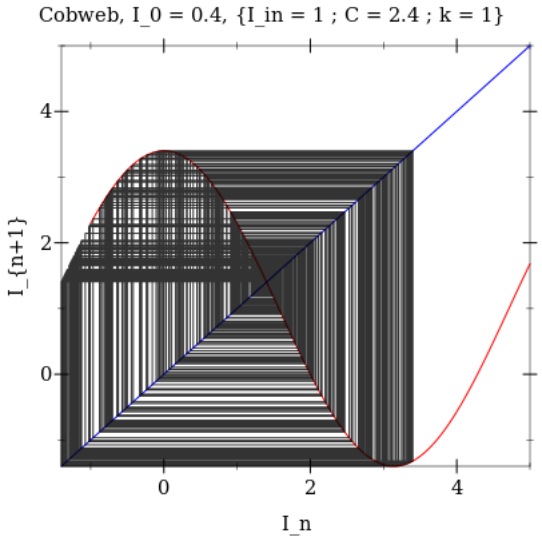

Figure 4: A cobweb diagram at $C = 2.4$ of the chaotic behavior that ensues above a threshold C value. The Liapunov exponent was calculated empirically to be $\lambda \approx 0.3937816 > 0$ and the derivative at each point visited to be $f'(x) > 1$, reinforcing the fact that this is a chaotic regime.

3.3 Orbit Diagram Analysis

A number of very surprising results appear in the orbit diagram calculation and analysis, see figure 5. The orbit diagram, while at times similar to the logistic map's orbit diagram, has stark differences.

First, we can see on the right plot of figure 5 that the 8-cycle branches leading to chaos briefly split into lobed $16-$cycle trajectories, something which provably doesn't occur in the logistic map. This is likely due to the non-unimodal nature of $1+\cos\theta$, which becomes greatly exaggerated as the nonlinear coefficient n_2 increases to an appreciable value. As an example of how unwieldy and unpredictable the orbit diagram can become in the case of strong nonlinearity, we calculated the orbit diagram when $n_2 = 10.0$ and find striking qualities in figure 6. A period-doubling sequence to chaos appears much sooner, with fully chaotic behavior occurring at $C \approx 0.22$, a full order of magnitude sooner than in the case of $n_2 = 1.0$. We can also see a jump from chaos to fully ordered behavior around $C \approx 0.27$, where another period-doubling sequence to chaos occurs. Finally, the lower branch of the previous chaotic regime appears and fills in the gap between itself and the new chaotic branch, producing a cone of chaos which continues for as far as we could calculate (with extremely short periodic regimes).

Second, we can see the appearance of artifacts in the descent to chaos, see figures 7 and 8. On many separate re-calculations of the orbit diagram we saw the appearance of separate stable yet unusual cycles that were "thick" in comparison to the true cycles appearing earlier in the period-doubling sequence. These thick cycles have periodic motion, although no point is visited twice in the trajectory. In the thick cycle shown, the cycle was found to have a Liapunov exponent $\lambda \approx -0.9997$ and a derivative product on the cycle to be $\Pi_i f'(x_i) \approx 0$, indicating super-stability! Thus we see the appearance of *two* stable cycles, one of which has "contained chaos," such that the trajectory never repeats itself. This is reminiscent of a strange attractor, where there is a qualitatively clear orbit that appears, but there exists chaotic behavior within the confines of the orbit.

Finally, we compare the I_{n+1} map to the logistic map in the case of small nonlinearity $n_2 = 0.05$. Since $\cos\theta \approx 1 - x^2/2$, we have that $I_{n+1} \approx (1 + C(1 - \frac{1}{2}x^2))$, which is a roughly unimodal map on its domain. The resulting comparison in figure 9 then shows that the universality theorems likely hold approximately for our nonlinear map as the orbit diagrams grow increasingly similar to each-other. This has an interesting implication: even in the case

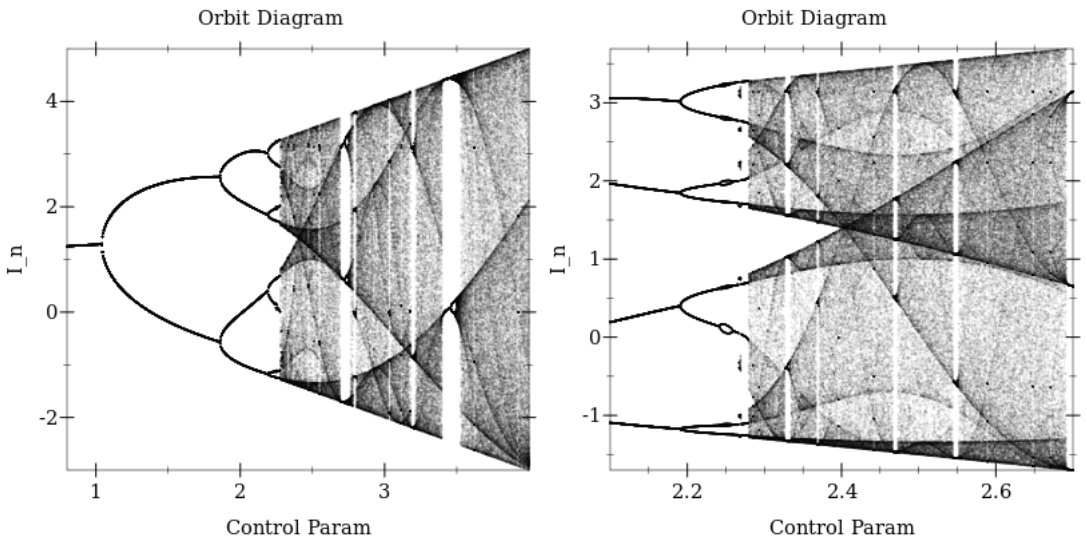

Figure 5: The orbit diagram for the I_{n+1} map. Chaos ensues at some critical C value around ≈ 2.3, but the situation is even less clear than in the logistic map case. On the right is a zoomed-in piece of the orbit diagram in the range $C \in [2.1, 2.7]$. In contrast to the logistic map, "lobes" appear briefly on each of the period-8 branches giving brief periods of period-16 cycles. Artifacts also appear for C ranges leading up to chaos, in this case an artifact appears around $C \approx 2.26$ where the branches of the orbit diagram are broken by streaks. This is investigated further in figure 7

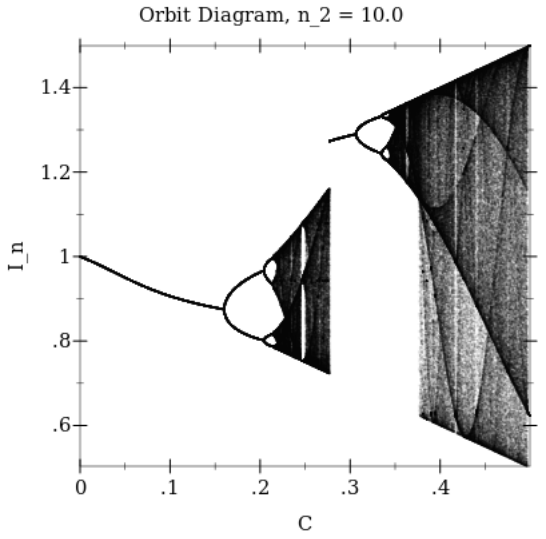

Figure 6: A calculation of an orbit diagram for the I_{n+1} map in the case of a very strong nonlinear coefficient $n_2 = 10.0$. First, chaos occurs much more quickly at around $C \approx 0.22$, a full order of magnitude smaller from $n_2 = 1.0$ with no change in the map's magnitude. Second, the chaos abruptly stops discontinuously around 0.27 to produce a second period-doubling sequence to chaos, where the lower branch of the previous chaotic portion re-appears and is "filled in" past a certain critical value $C \approx 0.355$, where chaos dominates for the forseeable future (with small periodic windows).

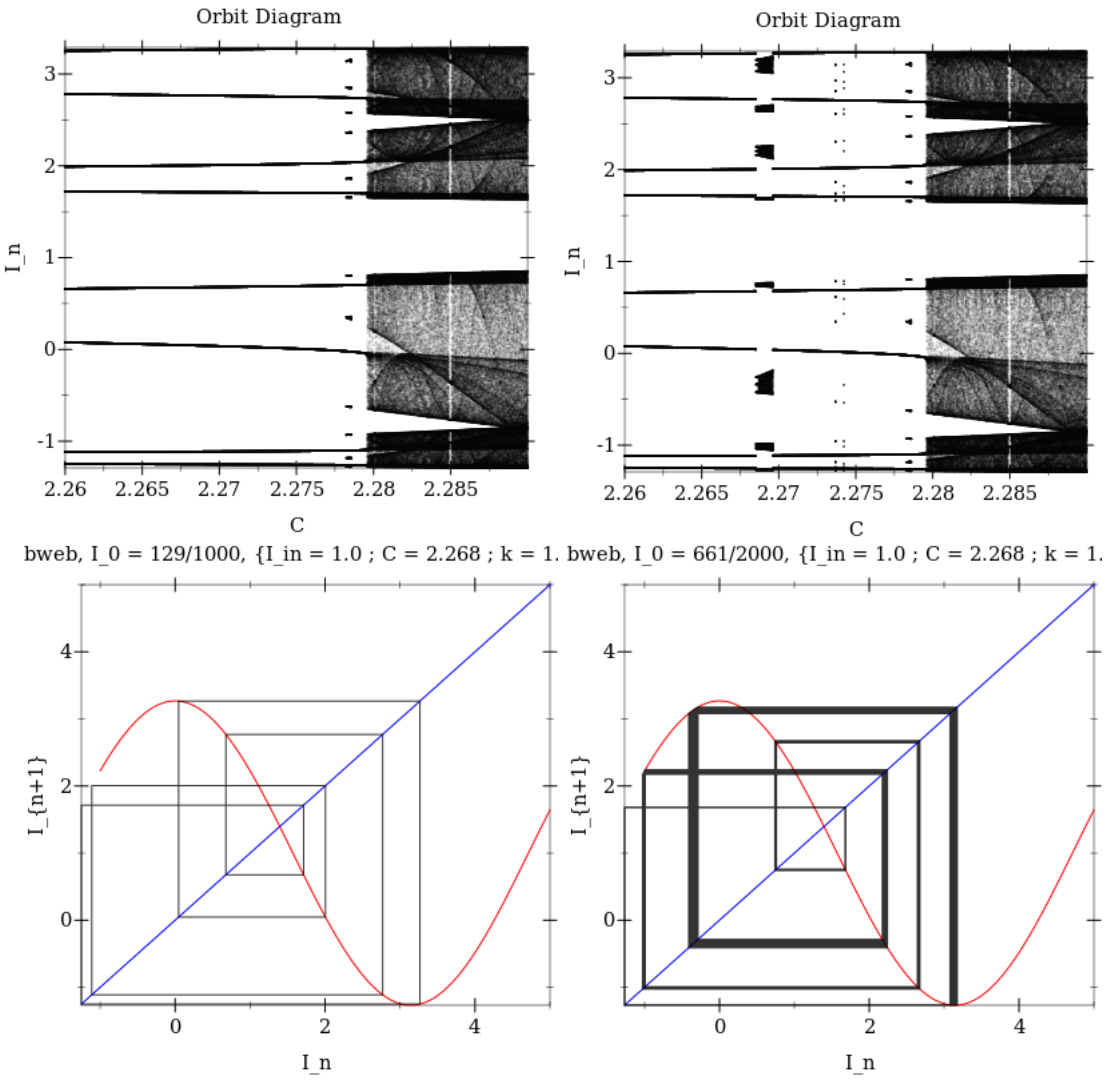

Figure 7: A close-up between an orbit diagram with few artifacts (left) and a separate orbit diagram calculation with thick and spotty artifacts (right) in the range $C \in [2.26, 2.29]$, as well as representative trajectories for the non-artifact and artifact trajectories appearing at $C = 2.268$ (bottom). The initial value of the map was chosen to be uniform in the range $I_0 \in [0, 2]$, leading to different *unique* asymptotic trajectories in very tight regions. The expected stable cycle trajectory appears on the left diagram, continuously connecting from the previous branches. Another "thick" trajectory shows itself periodically in the road to chaos, where the trajectory is roughly periodic but does not repeat itself and wobbles about separate cycle points, see figure 8 for a time-series of the thick trajectory.

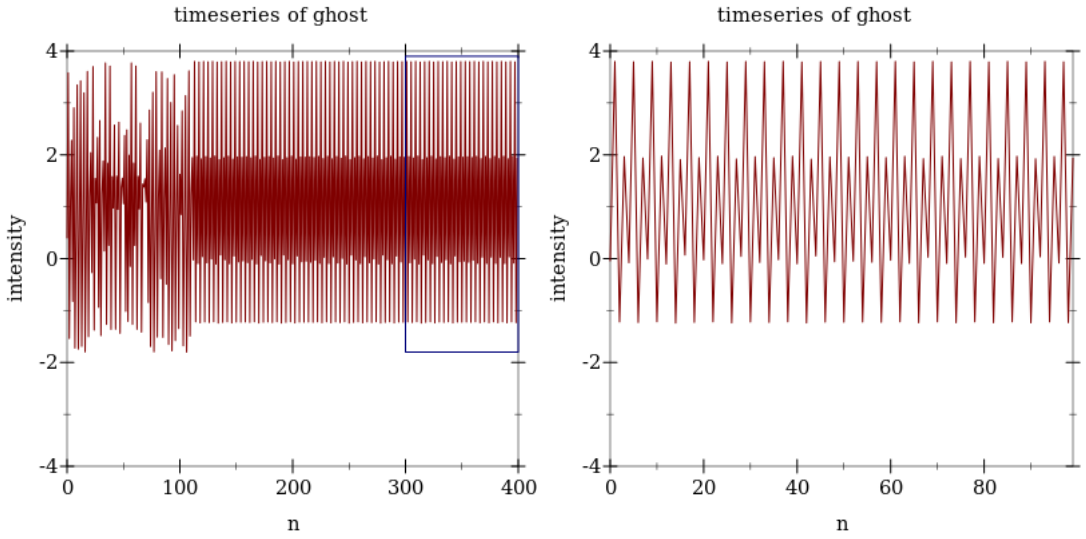

Figure 8: A time-series plot of the fat trajectory shown in the bottom-right of 7. On the left is the non-truncated trajectory and on the right is a zoom-in of the wobbling cycle demonstrated qualitatively by the cobweb diagram. No point is visited twice, giving a sense of "predictable chaos" or "bounded chaos" as in the case of the Lorenz map's strange attractor, although there is no bouncing *between* orbits in the finite-map case due to the stability of the thick orbit ($\lambda \approx -0.99997$ and $\Pi_i f(x_i) \approx 0$ indicating this is in fact a *super-stable* (thick) cycle!!)

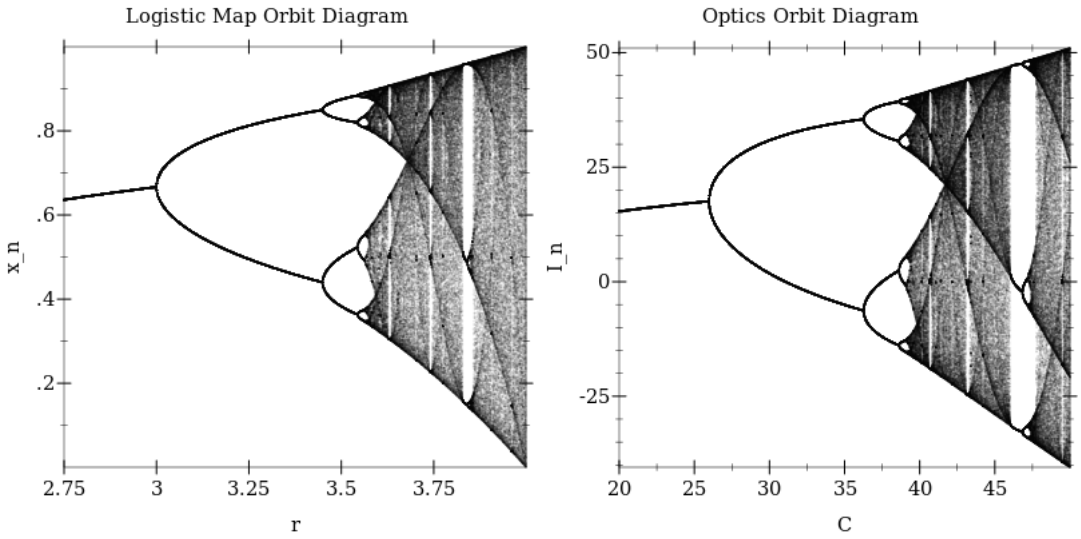

Figure 9: A comparison of the logistic map orbit diagram and the I_{n+1} orbit diagram in the case of very small nonlinearity, in this case $n = 0.05$. The result are two very similar orbit diagrams due to the fact that $\cos\theta$ expands into a quadratic when θ is small. The universality theorems for finite difference maps on unimodal distributions then apply, yielding qualitatively similar orbit diagrams.

of small nonlinearity in a dielectric medium, strong enough input intensity is *guaranteed* to produce chaos eventually by reduction to the logistic map, although the power levels required may be unrealistically and un-physically large.

3.4 (Complex) Chaos

We now return to the complex map. To turn the difference-differential equation pair into a difference map, we return to the adiabatic case of the above complex map, set $E_n = E(nt_R)$ so that our complex iterated map is

$$E_{n+1} = A + BE_n \exp\{i(|E_n|^2 - \phi_0)\}$$

We restrict ourselves to the case $\phi_0 = 0$ and $B = 0.4$ while varying A as in [4] and expand upon their analysis by calculating the fractal dimension for different values of A at the onset of chaos.

First, we confirm that we have a correct implementation of the complex map, shown in figure 10. The two generated sequences look qualitatively similar which is a good sign, allowing us to proceed. Notably, we produce around $30,000$ points for each of the generated plots below which opens the door for more precise fractal dimension calculations. We also plot points in the sequence with an opacity of 0.1 to emphasize roughly-uniform distribution of the map over the fractal. This allows us to say that the trajectories are truly chaotic, bouncing around in a seemingly random manner in the chaotic regime at a "uniform" rate, although regions of higher density of points appear due to the twisting of the fractal around certain bends and curves, for example the zoom-in of the fractal inner spiral in 12. We calculate the fractal dimension of each chaotic example by the procedure outlined in [7]: First, we generate a long series of points and remove the transient. Then we choose a sequence of $\epsilon_i > 0$. For each point on the trajectory $\mathbf{z}$, we then calculate $N_{\epsilon_i}(\mathbf{z})$, the number of neighbors of $\mathbf{z}$ within an ϵ_i-ball. For our case, we instead calculated an ϵ-box to speed up calculations since quadratic distances would have significantly slowed down this step. Finally, calculate the correlation $C(\epsilon_i) = \frac{1}{\#\text{ of points } \mathbf{z}} \sum_{\mathbf{z}} N_{\epsilon_i}(\mathbf{z})$. We then plot $\log \epsilon_i$ vs. $\log C(\epsilon_i)$ and get a rough slope, which approximates the correlation dimension of the fractal. Since the correlation dimension is bounded above by the fractal dimension, this should be a good enough measure for when we have something fractal-like. For the below, we need to be careful to choose each ϵ large enough to obtain an appreciable neighborhood of points but small enough so that the neighborhood doesn't cross over into different "twists" of the fractal. For this reason, we chose $\epsilon \in [0.01, 1.0]$. In practice, we approximate the above sum $\sum_{\mathbf{z}}$ by choosing 5000 random points of the generated map and averaging their neighborhood sizes, which should give reasonable approximation to $C(\epsilon)$ and significantly speed up calculation.

We chose three different complex iteration cases: $A = 2.0, 3.9$, and 10.0. These correspond to the cases of low chaos, "medium" chaos, and "high" chaos respectively, which is deemed qualitatively by how tightly the geometric object is being wound. In figure 11, we calculate the trajectory of the complex map to be a roughly 1-dimensional curve with signs of increasing dimension as we increase A. Next, we reproduce the fractal of figure 10 in figure 12 and find the correlation dimension to be roughly 1.41, a reasonable number. Finally, in the case of high-chaos when the geometric object is tightly and densely wound at $A = 10.0$, we still reach a correlation dimension of 1.41.

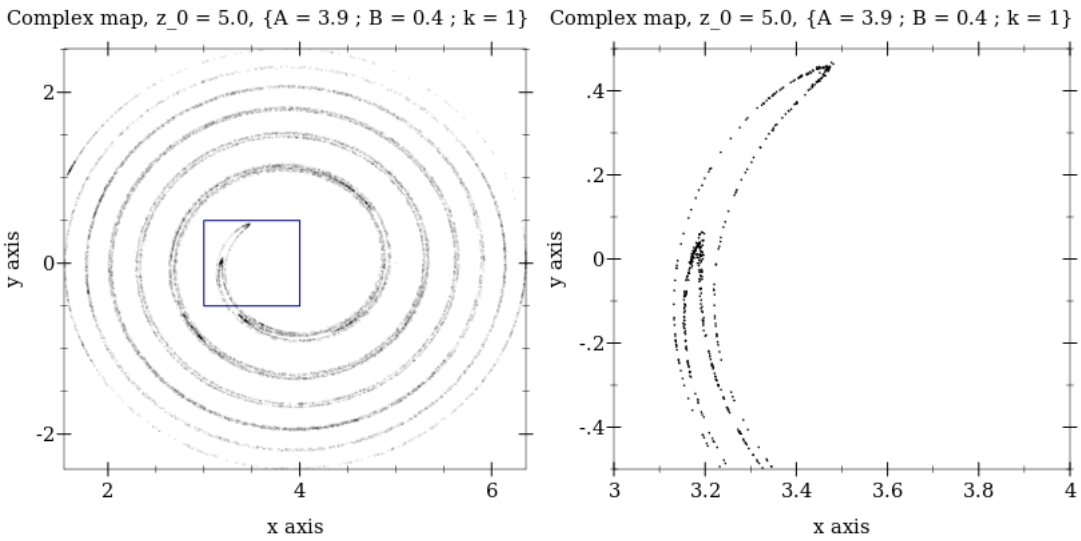

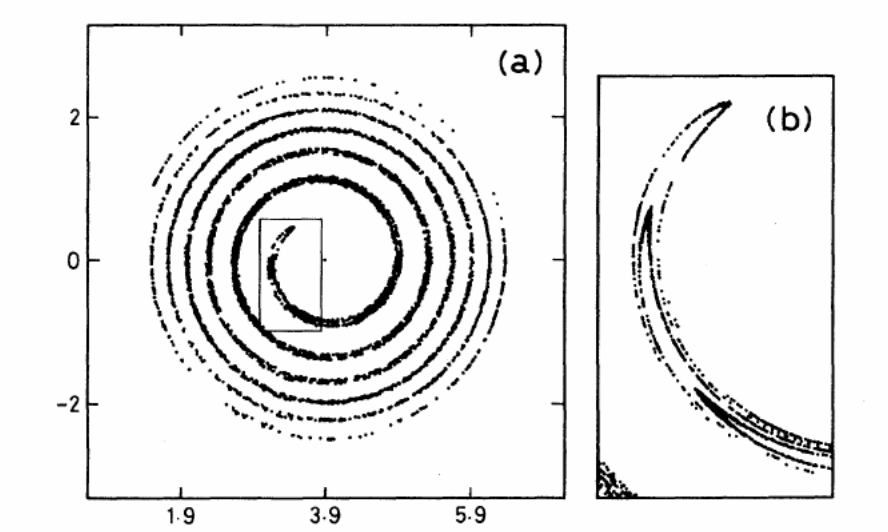

FIG. 2. (a) Plot of 5000 successive points of a series E_n on the complex E plane. The parameter values chosen are $B = 0.4$, $A = 3.9$, and $\varphi_0 = 0$. (b) Enlargement of the rectangular region of (a).

Figure 10: A comparison between our empirically calculated complex fractal and the fractal shown in [4]. Our fractal was calculated with 30,000 iterations of the complex map with an opacity of 0.1 given to each generated point, demonstrating qualitatively that the trajectory is chaotic and uniform over the attractor.

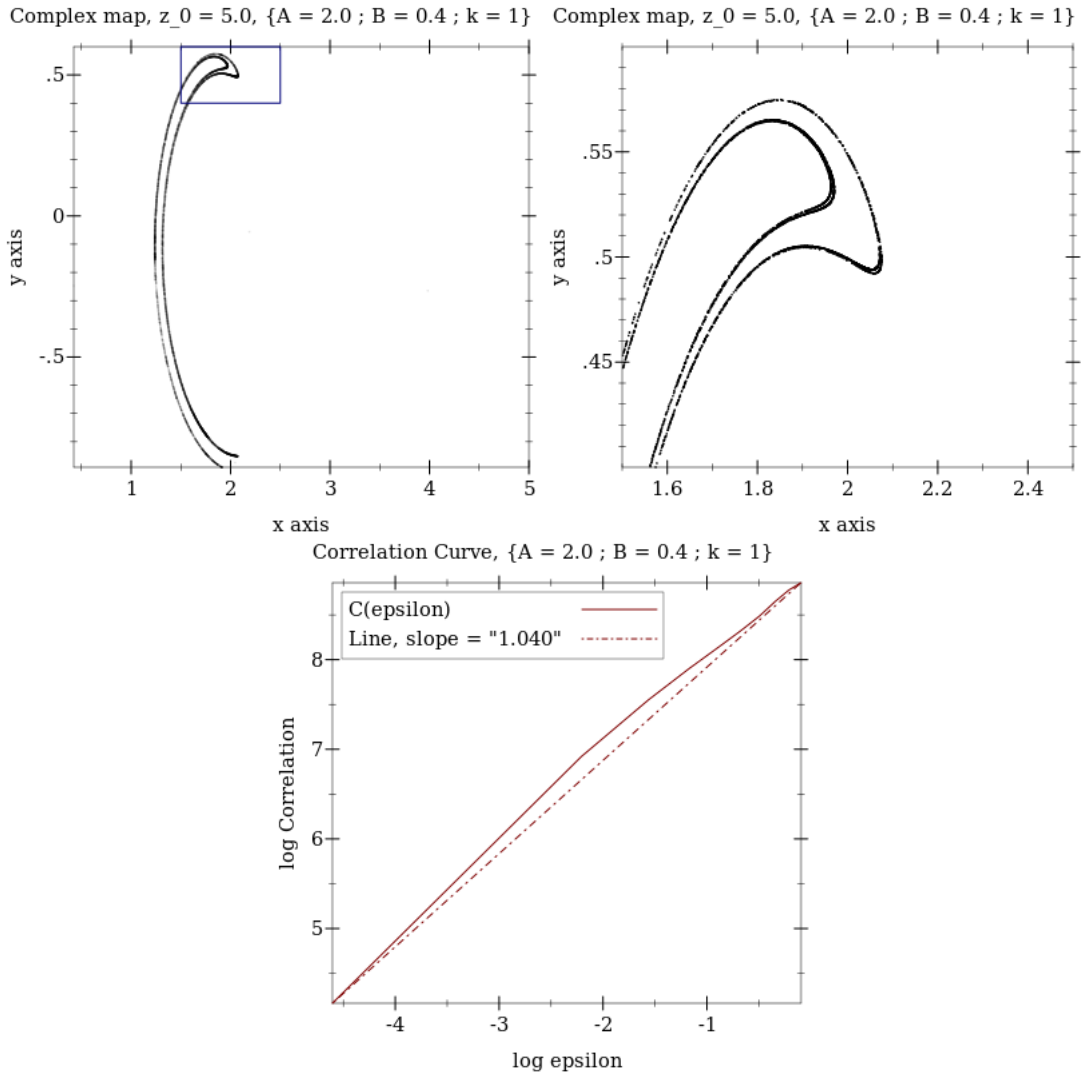

Figure 11: An example of early chaos in the complex map at $A = 2.0$. We calculate the fractal dimension to be barely above 1, which is supported qualitatively by a zoom-in on the fractal.

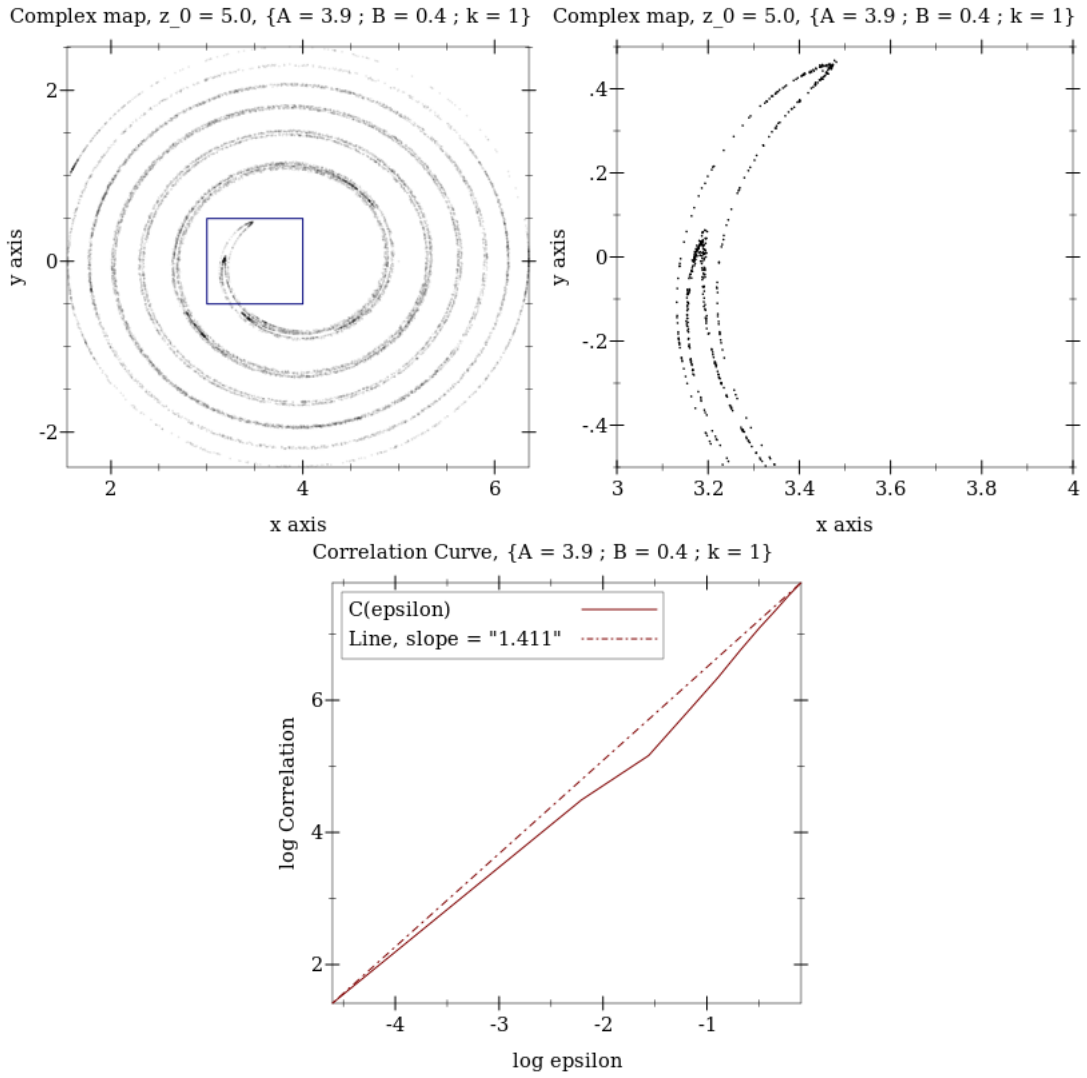

Figure 12: An example of mid-term chaos at $A = 3.9$, with the fractal in figure 11 being continually twisted into a spiral. We calculate the fractal dimension to be roughly 1.41.

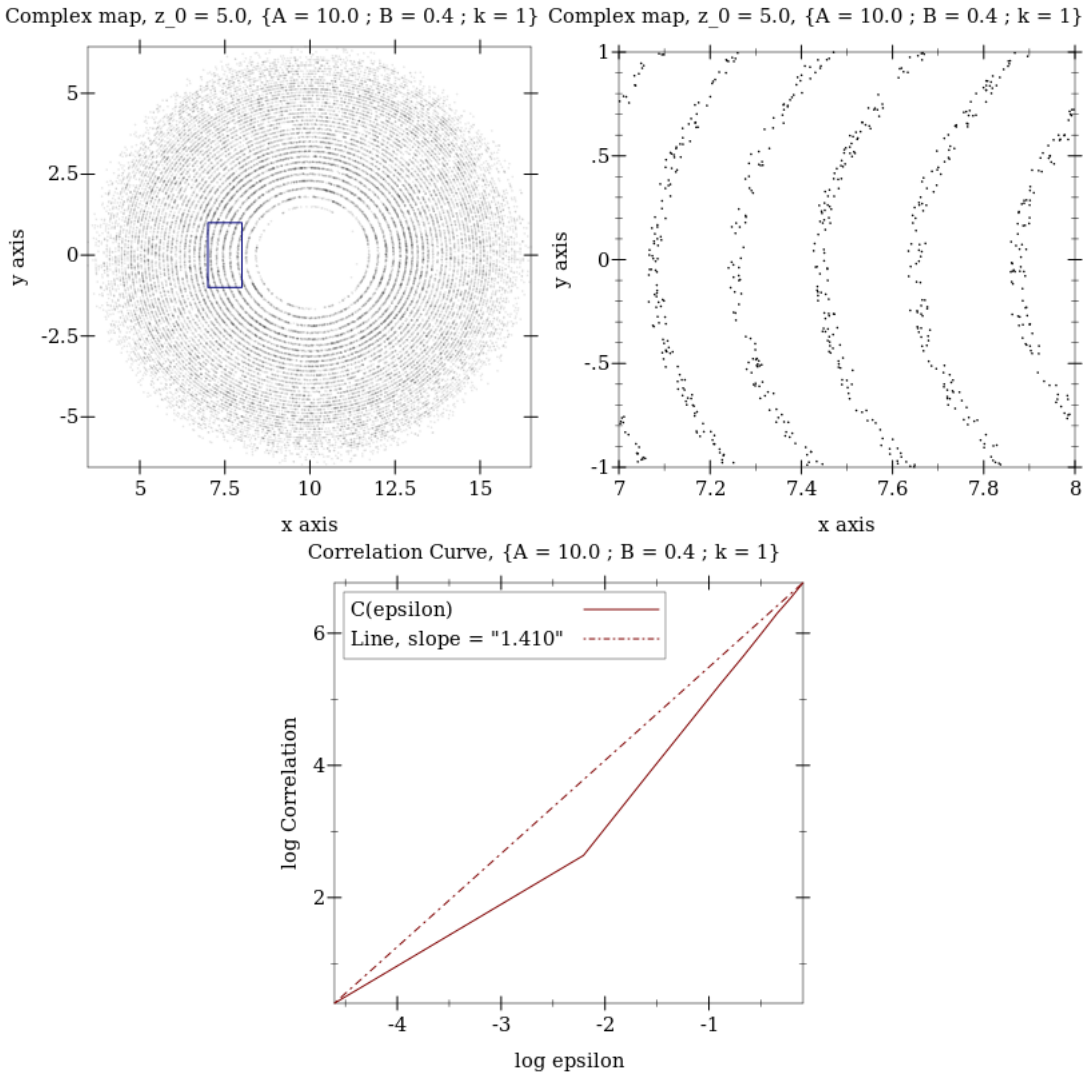

Figure 13: An example of late-term chaos at $A = 10.0$. Although the fractal is twisted into more densely packed spirals, the calculated dimension remains comparable to that of 12 at around 1.41.

4 Conclusions

We started by introducing a simple nonlinear effect in a dielectric medium in the ring resonator system. From this, clear chaos emerges at a high-intensity input field due to the system reducing to an iterated map in the adiabatic case $\gamma t_R \to \infty$, which allowed an analysis in either a complex iterated map of the field amplitude [4] or a real-valued map of the intensity [3]. The results are visually different but qualitatively related by chaos. In the case of the real map, we generated slices of the orbit diagram with important qualitative differences from the usual logistic and unimodal maps. These differences are then exacerbated as the nonlinear optical coefficient n_2 is increased further. We also found the coexistence of stable cycles with super-stable thick cycles, which have behavior reminiscent of a strange attractor whereby the thick trajectories have periodic motion but no repetition of the same points. In the case of the complex map, we generated sets of fractals and calculated the correlation dimension in each case, with the correlation dimension roughly saturating at ≈ 1.41.

References

[1] Robert W. Boyd. *Nonlinear Optics, Third Edition.* Academic Press, Inc., USA, 3rd edition, 2008.

[2] David J Griffiths. *Introduction to electrodynamics; 4th ed.* Pearson, Boston, MA, 2013. Re-published by Cambridge University Press in 2017.

[3] Robert G. Harrison and Dhruba J. Biswas. Chaos in light. *Nature*, 321(6068):394–401, May 1986. Number: 6068 Publisher: Nature Publishing Group.

[4] K. Ikeda, H. Daido, and O. Akimoto. Optical Turbulence: Chaotic Behavior of Transmitted Light from a Ring Cavity. *Physical Review Letters*, 45(9):709–712, September 1980. Publisher: American Physical Society.

[5] Kensuke Ikeda. Multiple-valued stationary state and its instability of the transmitted light by a ring cavity system. *Optics Communications*, 30(2):257–261, August 1979.

[6] Y. R Shen. *The principles of nonlinear optics*. J. Wiley, New York, 1984. OCLC: 10123484.

[7] Steven H. Strogatz. *Nonlinear Dynamics and Chaos: With Applications to Physics, Biology, Chemistry and Engineering*. Westview Press, 2000.